JBC RESEARCH ARTICLE

Calpain-mediated proteolytic production of free amino acids in vascular endothelial cells augments obesity-induced hepatic steatosis

Received for publication, October 28, 2021, and in revised form, April 2, 2022 Published, Papers in Press, April 18, 2022,
https://doi.org/10.1016/j.jbc.2022.101953

Risako Akasu[1], Takuro Miyazaki[1,*], Mohamed Z. Elhussiny[2,3], Yuki Sugiura[4], Yuki Tomitsuka[1], Shogo Haraguchi[1], Kinya Otsu[5], Vishwajit S. Chowdhury[2,6], and Akira Miyazaki[1]

From the [1]Department of Biochemistry, Showa University School of Medicine, Tokyo Japan; [2]Graduate School of Bioresource and Bioenvironmental Science, Kyushu University, Fukuoka, Japan; [3]Department of Animal & Poultry Behaviour and Management, Faculty of Veterinary Medicine, Aswan University, Aswan, Egypt; [4]Department of Biochemistry, Keio University School of Medicine, Tokyo, Japan; [5]The School of Cardiovascular Medicine and Sciences, King's College London British Heart Foundation Centre of Excellence, London, United Kingdom; [6]Faculty of Arts and Science, Kyushu University, Fukuoka, Japan

Edited by Qi-Qun Tang

Free amino acids that accumulate in the plasma of patients with diabetes and obesity influence lipid metabolism and protein synthesis in the liver. The stress-inducible intracellular protease calpain proteolyzes various substrates in vascular endothelial cells (ECs), although its contribution to the supply of free amino acids in the liver microenvironment remains enigmatic. In the present study, we showed that calpains are associated with free amino acid production in cultured ECs. Furthermore, conditioned media derived from calpain-activated ECs facilitated the phosphorylation of ribosomal protein S6 kinase (S6K) and *de novo* lipogenesis in hepatocytes, which were abolished by the amino acid transporter inhibitor, JPH203, and the mammalian target of rapamycin complex 1 inhibitor, rapamycin. Meanwhile, calpain-overexpressing capillary-like ECs were observed in the livers of high-fat diet–fed mice. Conditional KO of EC/hematopoietic *Capns1*, which encodes a calpain regulatory subunit, diminished levels of branched-chain amino acids in the hepatic microenvironment without altering plasma amino acid levels. Concomitantly, conditional KO of *Capns1* mitigated hepatic steatosis without normalizing body weight and the plasma lipoprotein profile in an amino acid transporter–dependent manner. Mice with targeted *Capns1* KO exhibited reduced phosphorylation of S6K and maturation of lipogenic factor sterol regulatory element–binding protein 1 in hepatocytes. Finally, we show that bone marrow transplantation negated the contribution of hematopoietic calpain systems. We conclude that overactivation of calpain systems may be responsible for the production of free amino acids in ECs, which may be sufficient to potentiate S6K/sterol regulatory element–binding protein 1–induced lipogenesis in surrounding hepatocytes.

Nonalcoholic fatty liver disease is frequently complicated by metabolic diseases, such as diabetes mellitus, dyslipidemia, and obesity (1). Nonalcoholic fatty liver disease ranges from mild steatosis to nonalcoholic steatohepatitis and can lead to cirrhosis and hepatocellular carcinoma; therefore, steatotic insult to the liver may cause life-threatening diseases. Many studies have focused on lipid handling in hepatocytes, including fatty acid uptake, *de novo* lipogenesis, and fatty acid oxidation. Mass spectrometry–based metabolomics analysis enables the investigation of crosstalk between metabolic organs. While symptomatic therapies, including insulin sensitization and lipid lowering, are applicable for the treatment of steatotic diseases (2), highly effective therapeutics for severe cases are currently unavailable.

Free amino acids, particularly branched-chain amino acids (BCAAs), accumulate in the plasma of patients with diabetes and obesity (3) and are mainly derived from skeletal muscle and the gut microbiome, which is associated with reduced fat-free mass (4). BCAAs can accelerate protein synthesis and increase in mass in skeletal muscle during exercise training and mitigate cachexia (4) and sarcopenia (5). In addition to their beneficial effects, BCAAs have deleterious effects in cardiometabolic diseases, including type 2 diabetes, obesity, and ischemic cardiovascular diseases (6). Previous studies have shown that plasma amino acids, including BCAAs, were elevated in patients with diabetes and positively correlated with plasma HbA1c levels (7). Accordingly, previous observational studies monitoring circulating BCAAs and intervention studies manipulating dietary BCAAs exhibited divergent experimental results in terms of changes in body composition and metabolism (5), likely because of their diverse metabolic roles and complicated crosstalk between organs. It was previously reported that transduction of the amino acid transporter, SNAT2, specifically led to augmented steatohepatitis (8), suggesting that excessive accumulation of amino acids in hepatocytes may cause hepatic steatosis. Most metabolic studies have focused on the systemic homeostasis of BCAAs, and the local production of amino acids in the liver microenvironment has not been fully elucidated.

Nonessential amino acids are biochemically synthesized during nutrient metabolism, including glycolysis and the citric

* For correspondence: Takuro Miyazaki, taku@pharm.showa-u.ac.jp.

© 2022 THE AUTHORS. Published by Elsevier Inc on behalf of American Society for Biochemistry and Molecular Biology. This is an open access article under the CC BY-NC-ND license (http://creativecommons.org/licenses/by-nc-nd/4.0/).

acid cycle. In addition to biogenic synthesis, amino acids can be generated by the proteolytic degradation of intracellular proteins *via* proteases. For instance, Atg7-mediated autophagy was shown to be required for sustaining intracellular-free amino acid levels in amino acid–starved cells (9). Proteasome inhibition in yeast, cells, and flies led to lethal amino acid shortage (10), suggesting that autophagy and proteasomes play a constitutive role in maintaining free amino acid levels in cells. In contrast to the constitutive proteolytic systems, some species of intracellular proteases are reportedly activated in response to extracellular stressors. We previously reported that calpain, an intracellular Ca^{2+}-dependent protease family, is activated during the pathogenic regulation of blood vessels (11–14). Among 15 species of isozymes, conventional calpains, which comprise heterodimers of calpain-1/calpain-s1 and calpain-2/calpain-s1, were disinhibited in vascular endothelial (VE) cells (ECs), thereby inducing pathological angiogenesis in retinopathy and cancer angiogenesis (15). Importantly, calpain proteases in ECs are reportedly activated in small vessels under diabetic conditions (16). Several enzymatic and biochemical investigations have reported that calpain recognizes many types of substrates, including the EC-marker VE-cadherin (17–19). Thus, it is speculated that activation of calpain leads to degradation of substantial amounts of proteins, producing excessive degradation products. It was recently reported that calpain-induced proteolysis facilitates proteasomal protein degradation (20). Therefore, we hypothesized that overactivation of calpain in ECs provides substantial amounts of free amino acids to the liver microenvironment under pathogenic conditions, which influences hepatic function.

The present study revealed that calpain proteolysis in cultured ECs is involved in the release of sufficient amounts of free amino acids, including BCAAs, to impact S6 kinase (S6K)/sterol regulatory element–binding protein 1 (SREBP1) pathway in neighboring hepatocytes, thereby inducing *de novo* lipogenesis. We generated EC/hematopoietic-specific and bone marrow–chimeric calpain-targeted mice to examine the contribution of EC calpain systems *in vivo*. Targeted inhibition of the EC calpain systems reduced BCAA levels in fatty liver independent of plasma amino acid levels and accompanying steatohepatitis in diet-induced obesity mice. This is the first study to identify local proteolytic amino acid production *via* stress-inducible intracellular proteases in the liver and define its pathophysiological roles in hepatic disorders.

Results

Effects of EC-derived amino acids on lipid handling in hepatocytes

Amino acids are hypothesized to leak from ECs in a process likely mediated by excessive calpain-induced proteolysis. Increased extracellular glucose levels led to elevation of a calpain-induced 95 kDa proteolytic fragment of VE-cadherin, which is a known calpain substrate, in human umbilical vein endothelial cells (HUVECs) within 15 min (Fig. 1*A*), indicating activation of conventional calpains in these cells at high glucose concentrations. Densitometry of total protein lysate showed that high–molecular weight proteins tended to be preferentially degraded in response to high glucose concentrations, whereas low–molecular weight proteins were sustained (Fig. 1*B*). Concomitantly, high glucose concentrations increased the amino acid levels in the culture supernatant, which plateaued within 15 min (Fig. 1*C*). Amino acid production at high glucose concentrations was greater than that at low glucose concentrations and was suppressed by calpeptin-induced pharmacological inhibition of calpain (Fig. 1*D*). Amino acid production is unlikely to be responsible for individual calpain substrates since it was unchanged when VE-cadherin was downregulated by siRNA (Fig. S1, *A* and *B*). We examined whether amino acid production was Ca^{2+} dependent using the Ca^{2+} ionophore, ionomycin. Supplementation of ionomycin to HUVECs resulted in degradation of intact VE-cadherin (125 kDa) and increased levels of calpain-generated 95 kDa fragments (Fig. 1*E*) and extracellular amino acid (Fig. 1*F*). Moreover, extracellular amino acid levels were decreased by inhibition of calpeptin-induced calpain but not bortezomib-induced proteasomal inhibition (Fig. 1*F*). Combined inhibition of calpain and proteasomes markedly reduced amino acid levels to lower than those in unstimulated cells. Luminometric assay revealed that treatment of HUVECs with ionomycin potentiated both calpain and proteasomal activity (Fig. 1, *G* and *H*). Calpain activity, but not proteasomal activity, was suppressed by siRNA-mediated silencing of *CAPNS1*, which encodes the common regulatory subunit of conventional calpains (Fig. 1, *G–I*). Since ionomycin-induced calcium influx limits protein ubiquitination in synapses (21), ubiquitination status was further examined in ionomycin-treated HUVECs (Fig. S1*C*). Consistent with previous reports, ionomycin treatment reduced expression levels of ubiquitinated protein in the cells within 30 min and was independent of pharmacological inhibition by bortezomib or calpeptin (Fig. S1*D*). The calpain dependency of individual amino acids was characterized using LC–tandem mass spectrometry (Fig. 1*J*). Levels of most amino acids, including BCAAs, detectable in the cell culture supernatants from ionomycin-stimulated HUVECs, were reduced by calpeptin treatment. Calpeptin-induced depletion of amino acid production was also observed in the murine MS1 EC line (Fig. 1*J*). Treatment of these cells with ionomycin upregulated intracellular BCAA levels in control cells (Fig. 1*K*), which was markedly inhibited by siRNA-mediated silencing of *CAPNS1*.

We investigated whether the products secreted from the calpain-activated ECs affected triglyceride homeostasis in hepatocytes using conditioned medium experiments. Carryover of ionomycin into the conditioned media was minimized by first stimulating ECs with ionomycin in the absence of extracellular Ca^{2+}, removing the ionomycin, and adding extracellular Ca^{2+} to the EC culture in the absence of serum or amino acids. This procedure activated calpain in ECs in the absence of ionomycin in the culture supernatant (Fig. 2*A*). Treatment of HepG2 hepatocytes cultured in vehicle-treated conditioned media with 100 nmol/l insulin failed to induce phosphorylation of S6K, whereas culturing HepG2 cells in

ASBMB

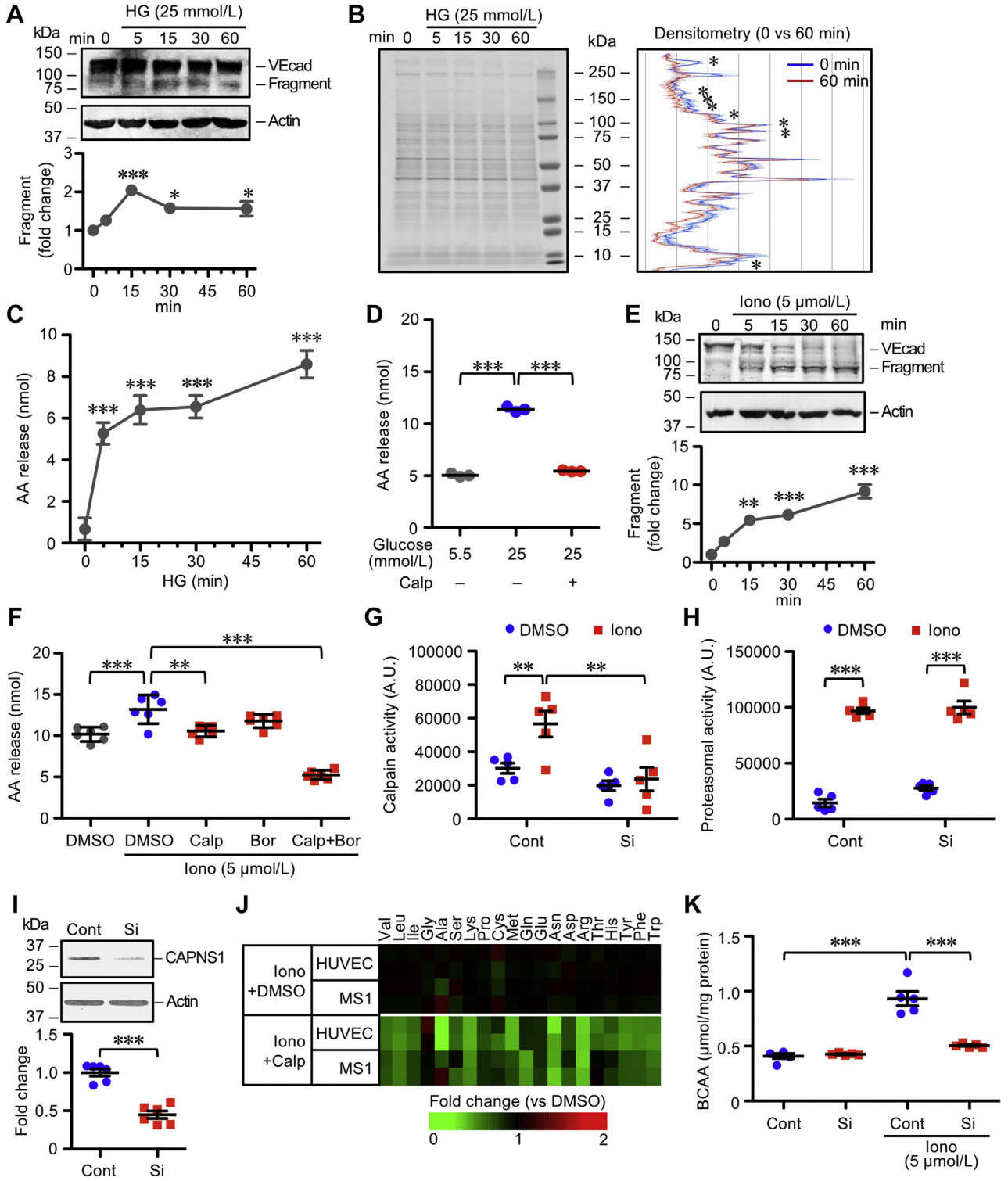

Figure 1. Calpain-induced BCAA production in cultured EC. *A*, high glucose–induced calpain activation in HUVECs. Proteolysis of VE-cadherin was monitored as an index of calpain activity. Cells were stimulated with high glucose (25 mmol/l) for the indicated periods. Relative expression of proteolytic fragment (95 kDa) *versus* intact VE-cadherin (125 kDa) is shown (n = 3). *B*, Coomassie brilliant blue staining of total protein lysate in HUVECs. Densitometric values at 60 min were averaged, and each peak was subjected to statistical analysis (n = 3). *C*, high glucose–induced amino acid release in HUVECs. Amino acid levels were quantified in the culture supernatant by biochemical assay (n = 5). *D*, pharmacological assessment of high glucose–induced amino acid release in HUVECs. Cells were pretreated with calpeptin at 10 μmol/l for 30 min and then incubated in Krebs–Henseleit buffer containing 25 mmol/l glucose in the presence of calpaptin. Amino acid levels in culture supernatant were measured (n = 3). *E*, ionomycin-induced calpain activation in HUVECs. Proteolysis of VE-cadherin was monitored as an index of calpain activity. Cells were stimulated with 5 μmol/l ionomycin for the indicated periods. Relative expression levels of proteolytic fragment (95 kDa) *versus* intact VE-cadherin (125 kDa) are shown (n = 3). *F*, pharmacological assessment of ionomycin-induced amino acid release in HUVECs. Cells were pretreated with 10 μmol/l calpeptin or 10 μmol/l bortezomib for 30 min and then incubated with 5 μmol/l ionomycin in the presence of inhibitor. Amino acid levels were measured in culture supernatant (n = 6). *G*, luminometric assay to measure calpain activity. Cells were incubated with 5 μmol/l ionomycin for 30 min. *H*, luminometric assay for measuring proteasomal activity. Cells were incubated with 5 μmol/l ionomycin for

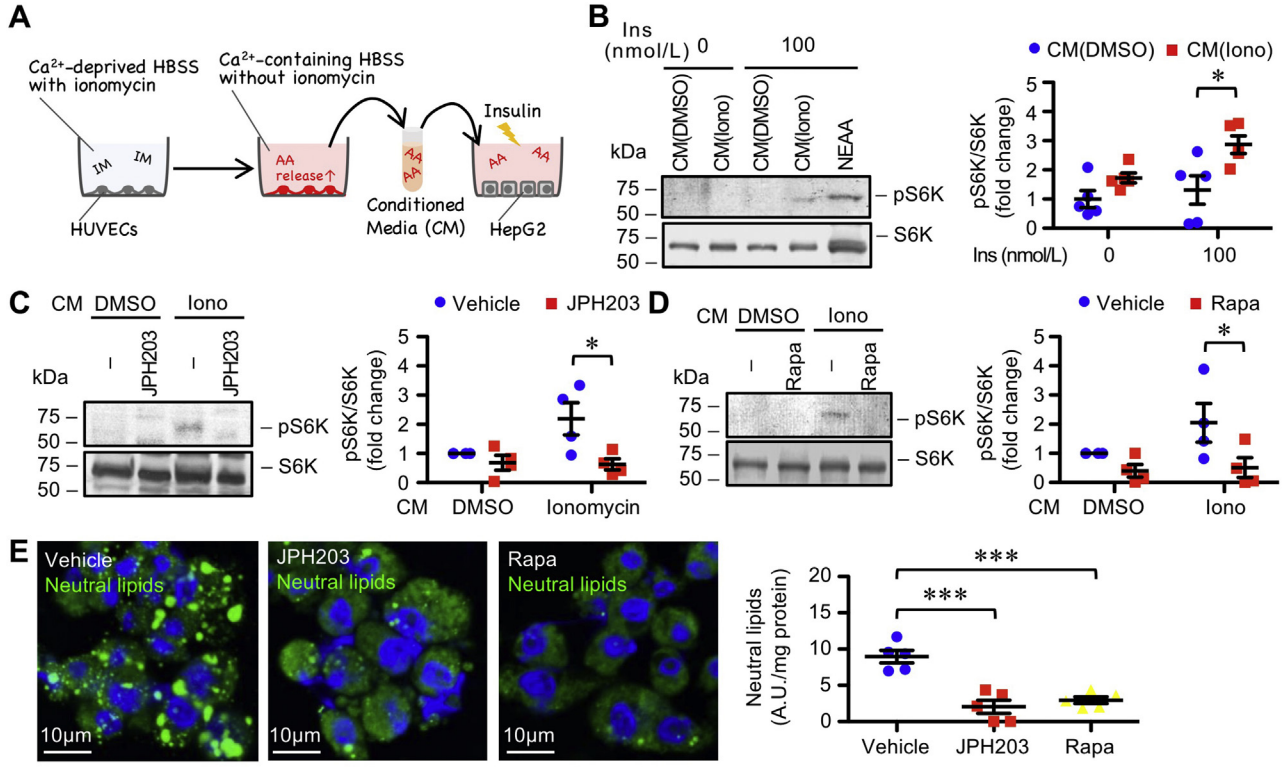

Figure 2. EC-derived amino acid is sufficient to induce lipid accumulation in hepatocytes. *A*, schematic illustration of conditioned media experiments. HUVECs were stimulated with ionomycin in Ca^{2+}-deprived HBSS. HBSS was then replaced with the Ca^{2+}-containing HBSS to induce Ca^{2+}-driven amino acid release from HUVECs in the absence of ionomycin in the extracellular environment. *B*, conditioned media experiments in HepG2 cells. Conditioned media derived from ionomycin-treated HUVECs amplified insulin-induced phosphorylation of S6K in HepG2 cells (n = 5). *C*, pharmacological assessment of amino acid transporter. About 50 nmol/l JPH203 was added to the HepG2 culture 30 min prior to insulin treatment (n = 4). *D*, pharmacological assessment of mTOR signaling. About 10 nmol/l rapamycin was added to the HepG2 culture 30 min prior to insulin treatment (n = 4). *E*, pharmacological assessment of *de novo* lipogenesis in HepG2 cells in response to conditioned media. About 50 nmol/l JPH203 or 10 nmol/l rapamycin were added to the HepG2 culture 30 min prior to insulin treatment. Cells were incubated with medium containing 100 nmol/l insulin and 0.05 mg/ml palmitic acid for 24 h (n = 5). Statistical analysis was performed using one-way ANOVA with Bonferroni post hoc test (*E*) and two-way ANOVA with Bonferroni post hoc test (*B–D*). *$p < 0.05$ and ***$p < 0.001$. EC, endothelial cell; HBSS, Hank's balanced salt saline; HUVEC, human umbilical vein endothelial cell; mTOR, mammalian target of rapamycin; S6K, S6 kinase.

ionomycin-treated conditioned media markedly upregulated S6K phosphorylation in response to insulin (Fig. 2*B*). S6K phosphorylation could be reproduced by adding leucine alone, instead of conditioned medium (Fig. S2, *A–C*). We then investigated the contribution of amino acids in the conditioned media and mammalian target of rapamycin complex 1 (mTORC1) in hepatocytes to S6K phosphorylation. Treatment of HepG2 hepatocytes with the L-type amino acid transporter 1 (LAT1) inhibitor, JPH203 (Fig. 2*C*) (22), and mTORC1 inhibitor, rapamycin (Fig. 2*D*) (23), clearly downregulated insulin-induced S6K phosphorylation in the ionomycin-treated conditioned media, whereas S6K phosphorylation in the vehicle control groups was unaffected even in the presence of these inhibitors. Consistently, insulin-induced *de novo* lipogenesis in HepG2 hepatocytes in ionomycin-treated conditioned media was clearly downregulated by JPH203 and rapamycin (Fig. 2*E*).

Targeting calpain systems in vascular ECs ameliorates hepatic steatosis

Obesity and steatohepatitis were induced in mice fed a high-fat diet (HFD) for 18 weeks compared with mice fed a low-fat diet (LFD). HFD-fed mice showed weight gain compared with LFD-fed mice (LFD: 23.3 ± 0.3 g, n = 18; HFD: 38.1 ± 1.0 g, n = 12; $p < 0.001$). Previous studies reported that expression levels of CD31 in sinusoidal ECs under physiological conditions were reportedly lower than those in other EC types, including heart, lung, and kidney ECs (24), and that $CD31^+$ capillary-like ECs were present in HFD-induced steatohepatitis (25). Consistently, $CD31^+$ capillary-like ECs were observed in murine liver after HFD feeding (Fig. S3*A*). Expression levels of the capillary-like EC markers, *Pecam1* and *Cd34*, were upregulated in HFD-fed mice compared with LFD-fed mice (Fig. S3*B*). Furthermore, calpain-s1-overexpressing cells were observed and clearly overlapped

30 min. *I*, siRNA-mediated silencing of *CAPNS1* in HUVECs. Immunoblot analysis was performed to examine the efficacy of siRNA (n = 3). *J*, amino acid composition in supernatants in HUVECs and murine MS1 cell culture. Cells were stimulated with 5 μmol/l ionomycin in the presence or the absence of 10 μmol/l calpeptin. Culture supernatant was analyzed in duplicate by liquid chromatography–tandem mass spectrometry. *K*, ionomycin increased the calpain-induced BCAA content in HUVECs. BCAA assay was performed in cell lysates (n = 5). Statistical analysis was performed using one-way ANOVA with Bonferroni post hoc test (*A*, *C–F*), two-way ANOVA with Bonferroni post hoc test (*G*, *H*, and *K*), and two-tailed Student's *t* test (*B*, *I*, and *J*). *$p < 0.05$, **$p < 0.01$, and ***$p < 0.001$. BCAA, branched-chain amino acid; EC, endothelial cell; HUVEC, branched-chain amino acid; VE, vascular endothelial.

with CD31 (Fig. 3*A*), whereas CD31 and calpain-s1 expression were not seen in LFD-fed mice. Furthermore, $CD31^+$ cells in HFD-fed mice simultaneously expressed calpain-1 (Fig. 3*A*). The specificity of CD31 immunostaining was confirmed in the microvessels of pancreatic islets (Fig. S3*C*). The EC fraction was isolated from the liver, and immunoblotting revealed that calpain-s1 was consistently upregulated in the liver EC fraction (Fig. 3*B*). Quantitative real-time PCR (qRT–PCR) analysis suggested that HFD feeding potentiates the expression levels of *Capns1* (calpain-s1 gene) in liver, whereas *Capns1* expression levels remained unchanged in skeletal muscle and adipose tissue (Fig. 3*C*).

Calpain-s1 is a common regulatory subunit of conventional calpain systems that stabilizes the catalytic subunits, calpain-1 and calpain-2. We examined the effects of targeted conditional KO (cKO) of *Capns1* to abolish conventional calpain activity in HFD-fed mice. CD31 is reportedly expressed in several hematopoietic cell lineages as well as ECs (26). Accordingly, *Capns1* was targeted in ECs and hematopoietic cells using the Tie2 promotor and Cre/loxP recombination systems, since the Tie2 promoter is functional in these cells (27). Protein expression levels of calpain-s1 in the liver EC fraction were successfully eliminated by conditional recombination (Fig. 3*D*). The calpain-induced proteolytic fragment of VE-cadherin, which is an EC-specific calpain substrate (19), was consistently reduced in the EC fraction by targeted KO of *Capns1*. This suggests that KO of *Capns1* eliminates the activity of conventional calpains in the cells.

Steatogenic phenotypes in the liver were also explored. Histological analysis and Oil Red O staining revealed several lipid droplets and diffuse lipid accumulation in the liver parenchyma in HFD-fed $Capns1^{fl/fl}$ mice, which were shrunk and reduced by EC/hematopoietic *Capns1* KO (Fig. 3*E*). Consistent with this findings, hepatic triglyceride levels were substantially reduced by *Capns1* KO (Fig. 3*F*). EC/hematopoietic cell-specific transgenic induction of *CAST* was performed to downregulate the conventional calpain systems in cells (15) and evaluated in terms of obesity-induced steatosis. Hepatic triglyceride levels in *CAST* conditional transgenic (cTg) mice were lower than those in the control mice (LNL–*CAST* Tg mice) (Fig. 3*G*). Bone marrow transplantation was performed to elucidate the contribution of hematopoietic calpains to lipid accumulation. PCR-based genotyping of bone marrow cells indicated successful chimerism in animals that underwent hematopoietic cell transplant (Fig. 3*H*). Chimeric mice were then subjected to HFD feeding for 18 weeks. The reduction of triglycerides in the liver was not reproduced in chimeric *CAST* cTg mice (Fig. 3*I*), negating the contribution of hematopoietic calpain systems to hepatic steatosis. HPLC-based lipoprotein profiling showed that plasma triglyceride and cholesterol levels were comparable between HFD-fed $Capns1^{fl/fl}$ and EC/hematopoietic *Capns1* cKO mice (Figs 3*I* and S3*D*). In contrast to the lipid deposition in the liver, the fibrogenic responses in the HFD-fed $Capns1^{fl/fl}$ and cKO mice were comparable (Fig. S3, *E* and *F*), likely because of the moderate fibrogenic responses in our experimental models. HFD-induced $CD31^+$ ECs were detectable in liver even in $Capns1^{fl/fl}$ and cKO mice (Fig. S3*G*). Furthermore, there were no differences in expression levels of the capillary-like EC markers, *Pecam1* and *Cd34*, as well as *Cdh5* (VE-cadherin gene) between $Capns1^{fl/fl}$ and cKO mice (Fig. S3*H*).

Hepatic lipogenic signaling and microenvironmental amino acids are disturbed by calpain systems in vascular ECs

We characterized the composition of amino acids in liver in HFD-fed mice. Among the 19 amino acids measured, HPLC-based quantification of amino acids showed that leucine, isoleucine, and glycine were reduced in HFD-fed EC/hematopoietic *Capns1* cKO mice compared with $Capns1^{fl/fl}$ mice (Figs. 4*A* and S4*A*). Biochemical analyses revealed reduced hepatic BCAA levels because of cKO of *Capns1* in HFD-mice (Fig. 4*B*), whereas plasma BCAA levels were unchanged when the conventional calpain systems were targeted (Fig. 4*C*). Reduced hepatic BCAA levels could be reproduced in HFD-fed EC/hematopoietic *CAST* cTg mice compared with controls (Fig. 4*D*). Of note, bone marrow transplantation revealed that the hematopoietic portion of the calpain system was not associated with changes in BCAAs (Fig. 4*E*). The isolated EC fraction from murine liver was compared with isolated bone marrow macrophages in terms of amino acid production (Fig. 4, *F* and *G*). Treatment of *Capns1* floxed cells with high glucose concentrations resulted in increase in amino acid levels in the cell culture supernatant. This was inhibited by targeted KO of EC/hematopoietic *Capns1*. In contrast, high glucose concentration did not facilitate amino acid production in isolated bone marrow–derived macrophages, which was independent of *Capns1* expression levels.

Obesity and diabetes parameters were further investigated. Targeted depletion of calpain-s1 or transgenic overexpression of calpastatin specifically in ECs and hematopoietic cells did not affect body weight gain in HFD-fed mice over 18 weeks (Fig. S5, *A* and *B*). Intraperitoneal glucose tolerance tests showed that HFD-fed $Capns1^{fl/fl}$ mice exhibited elevated blood glucose levels in response to intraperitoneal glucose injection (Fig. S5*C*). While targeted *Capns* knockdown slightly interrupted the initial elevation in plasma glucose, the areas under the curve of the $Capns1^{fl/fl}$ and cKO mice were comparable. In contrast, *Capns1* cKO ameliorated insulin resistance in HFD-fed mice (Fig. S5*D*). Similar trends in glucose and insulin tolerance were observed in *CAST* cTg and control mice (Fig. S5, *E* and *F*). In contrast, there were no differences in glucose and insulin tolerance between the LFD-fed $Capns1^{fl/fl}$ and cKO mice (Fig. S5, *G* and *H*). It is important to note that pancreatic insulin production was not substantially perturbed since plasma insulin levels in $Capns1^{fl/fl}$ and cKO mice were equivalent between fasting and fed conditions (Fig. S5*I*). Bone marrow transplantation indicated that glucose (Fig. S5*J*), insulin resistance (Fig. S5*K*), and body weight gain (Fig. S5*L*) in response to HFD feeding were not influenced by hematopoietic calpain targeting in chimeric mice; thus, it was concluded that EC calpain systems were responsible for insulin sensitization.

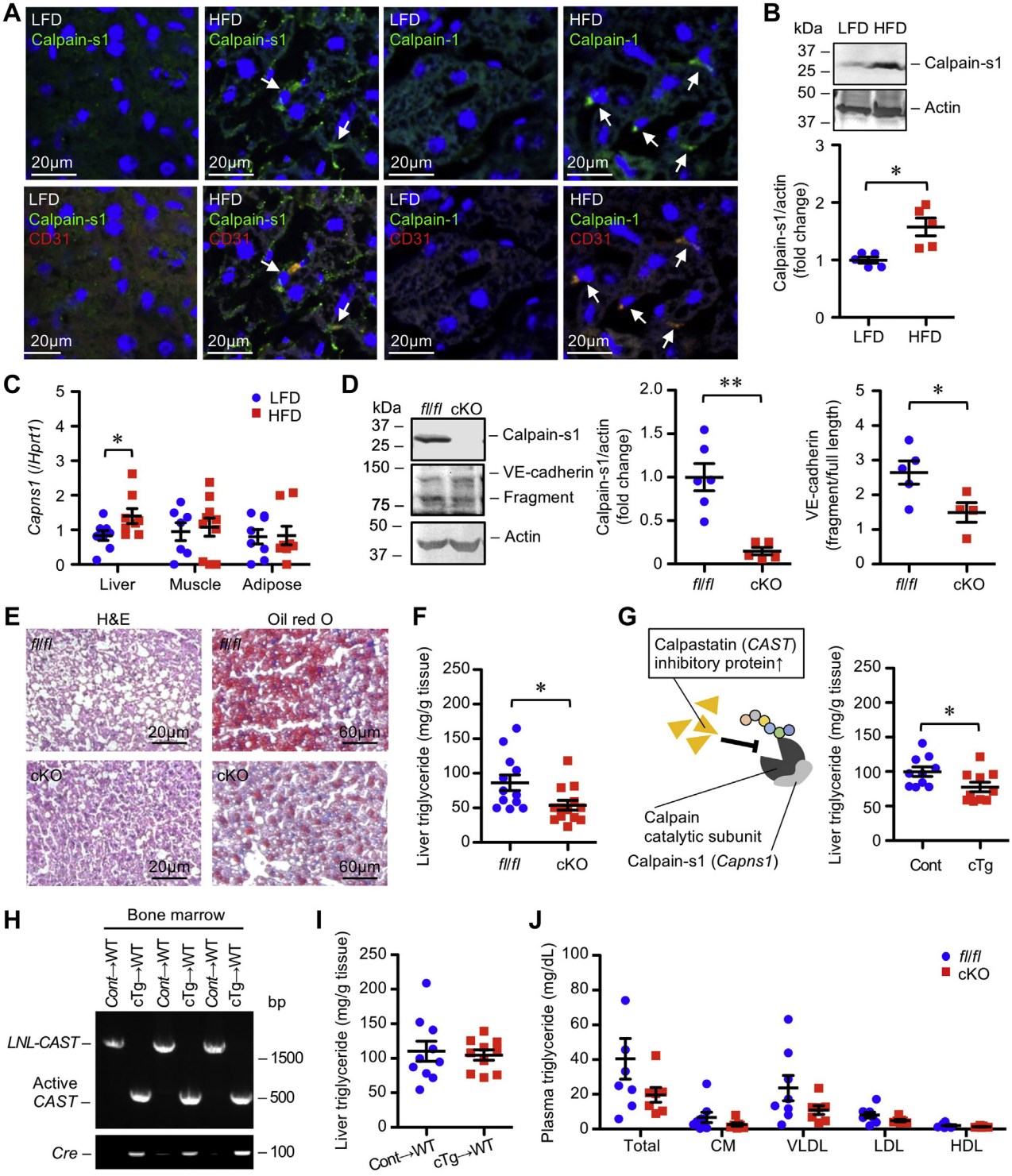

Figure 3. Targeted knockdown of endothelial calpain systems ameliorates hepatic steatosis without altering plasma triglyceride levels. Mice were fed an HFD for 18 weeks. *A*, localization of conventional calpains in liver from LFD- or HFD-fed mice. Immunohistochemical analysis was performed in liver parenchyma. *Arrows* represent CD31$^+$ calpain-1$^+$ cells. *B*, upregulation of calpain-s1 in the EC fraction in the livers of LFD- or HFD-fed mice. The liver EC fraction was isolated according to specific gravity and adhesiveness (n = 5). *C*, *Capns1* expression in metabolic organs in obese mice (liver, LFD: n = 8, HFD: n = 8; muscle, LFD: n = 7, HFD: n = 10; adipose tissue, LFD: n = 8, HFD: n = 8). *D*, protein expression of calpain-s1 and its substrate VE-cadherin in hepatic endothelial fractions in HFD-fed *Capns1*-targeted mice. Deficiency of calpain-s1 reportedly destabilizes catalytic subunits, thereby declining proteolytic activity. *Right graph* represents densitometry of immunoblot data (*Capns1 fl/fl*: n = 6, cKO: n = 5; VE-cadherin *fl/fl*: n = 5, cKO: n = 4). *E*, hematoxylin and eosin (*left*) and Oil Red O staining (*right*) of fatty liver sections of HFD-fed *fl/fl* or *Capns1*-targeted mice. *F*, triglyceride levels in liver were decreased by endothelial/hematopoietic-specific calpain targeting. Triglyceride content in HFD-fed mice was measured by biochemical assay and normalized to liver weight (*fl/fl*: n = 12; cKO: n = 13). *G*, overexpression of endogenous calpain inhibitor in EC/hematopoietic cells can mitigate hepatic steatosis. EC/hematopoietic cell–specific *CAST* cTg mice were generated by intercrossing LNL–*CAST* Tg mice with *Tie2–Cre* Tg mice (*left*). LNL–*CAST* Tg mice were used as a control (cont). The triglyceride content per liver weight in HFD-fed mice was measured (cont: n = 10; cTg: n = 10). *H*, genotype in bone marrow–chimeric mice. PCR-based genotyping was conducted in isolated bone marrow cells (n = 3). *I*, conventional calpains in hematopoietic cells are dispensable for hepatic steatosis.

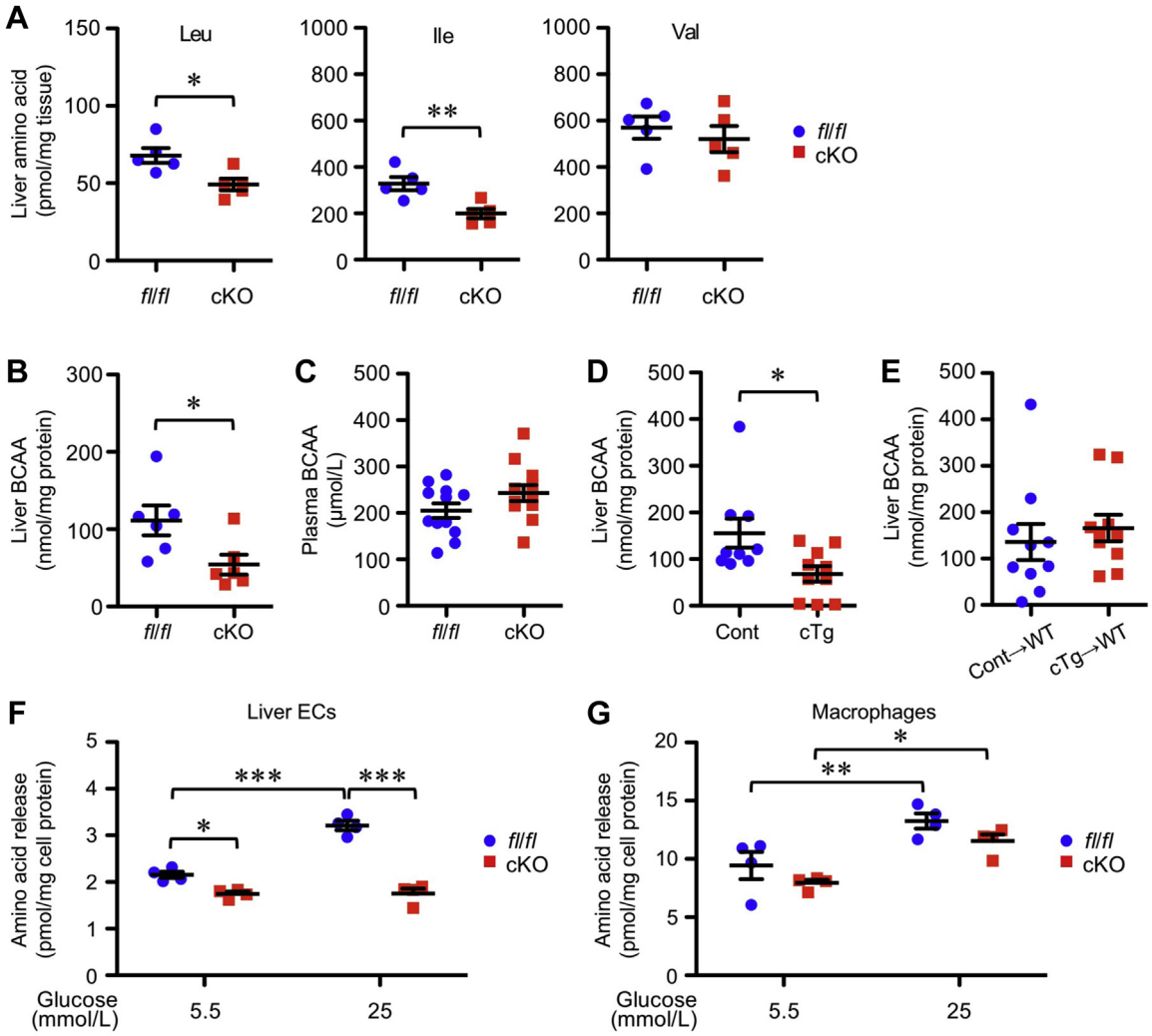

Figure 4. Conventional calpains in vascular ECs influence amino acid composition in liver of HFD-fed mice. Mice were fed an HFD for 18 weeks. *A*, BCAA levels in fatty liver in the HFD-fed endothelial/hematopoietic-specific *Capns1*-targeted mice. Amino acids were quantified by HPLC analysis (*fl/fl*: n = 5; cKO: n = 5). *B*, BCAA content in fatty liver in HFD-fed EC/hematopoietic-specific *Capns1*-targeted mice. BCAA was measured by biochemical assay (*fl/fl*: n = 6; cKO: n = 6). *C*, plasma BCAA levels in the HFD-fed endothelial/hematopoietic-specific *Capns1*-targeted mice (*fl/fl*: n = 12; cKO: n = 12). *D*, BCAA content in liver from HFD-fed EC/hematopoietic-specific *CAST* tg mice (cont: n = 9; cTg: n = 10). *E*, BCAA content in fatty liver from the HFD-fed chimeric *CAST* cTg mice (cont→WT: n = 10; cTg→WT: n = 10). *F*, amino acid release from isolated liver ECs. Cells were stimulated with high glucose concentrations at 25 mmol/l (*fl/fl*: n = 4; cKO: n = 4). *G*, amino acid release from isolated liver bone marrow–derived macrophages. Cells were stimulated with high glucose concentrations of 25 mmol/l (*fl/fl*: n = 4; cKO: n = 4). Statistical analysis was performed using two-tailed Student's *t* test (*A*, *B*, and *D*) and two-way ANOVA with Bonferroni post hoc test (*F*). $*p < 0.05$, $**p < 0.01$. BCAA, branched-chain amino acid; cKO, conditional KO; EC, endothelial cell; HFD, high-fat diet.

Next, AKT phosphorylation in metabolic organs was examined to elucidate the causal relationship between hepatic steatosis and insulin sensitization. In contrast to the hepatic steatotic phenotypes, AKT phosphorylation in the liver and skeletal muscle was equivalent between EC/hematopoietic *Capns1* $^{fl/fl}$ and *Capns1* cKO mice (Fig. 5, *A* and *B*), whereas AKT phosphorylation in adipose tissue was significantly upregulated by targeted *Capns1* knockdown (Fig. 5*C*). AKT signaling effectors were further examined, and expression levels of the gluconeogenesis-related effector, *Foxo1*, were consistently suppressed by *Capns1* KO in the adipose tissue of obese mice (Fig. S5*M*). In contrast, phosphorylation of FOXO1 (Fig. S5*N*) and its expression levels (Fig. S5*M*) in liver were comparable between EC/hematopoietic *Capns1* $^{fl/fl}$ and *Capns1* cKO mice. On the other hand, expression levels of the *de novo* lipogenesis-related effector, *Srebf1* (SREBP1 gene), were unchanged in adipose tissue but significantly down-regulated in liver in response to targeted KO of *Capns1* (Fig. S5*O*). SREBP1 is translated as an immature precursor and proteolytically converted into its active mature form (mSREBP1) (28). Immunoblotting showed that the maturation of SREBP1 in the livers of obese mice was reduced in response to *Capns1* KO (Fig. 5*D*), whereas mSREBP1 levels in skeletal muscle and adipose tissue were unaffected (Fig. 5, *E* and *F*).

Control or *Capns1* cTg donor mice and *Ldlr*$^{-/-}$ recipient mice (WT) were fed an HFD for 18 weeks. Triglyceride content per liver weight was measured (cont: n = 10; cTg: n = 10). *J*, plasma lipid profile in HFD-fed hematopoietic/EC–*Capns1* cKO mice. EDTA plasma was analyzed by HPLC (*fl/fl*: n = 8; cKO: n = 7). Statistical analysis was performed using two-tailed Student's *t* test (*B–D*, *F*, and *G*). $*p < 0.05$, $**p < 0.01$. cKO, conditional KO; cTg, conditional transgenic; EC, endothelial cell; HFD, high-fat diet; LFD, low-fat diet; VE, vascular endothelial.

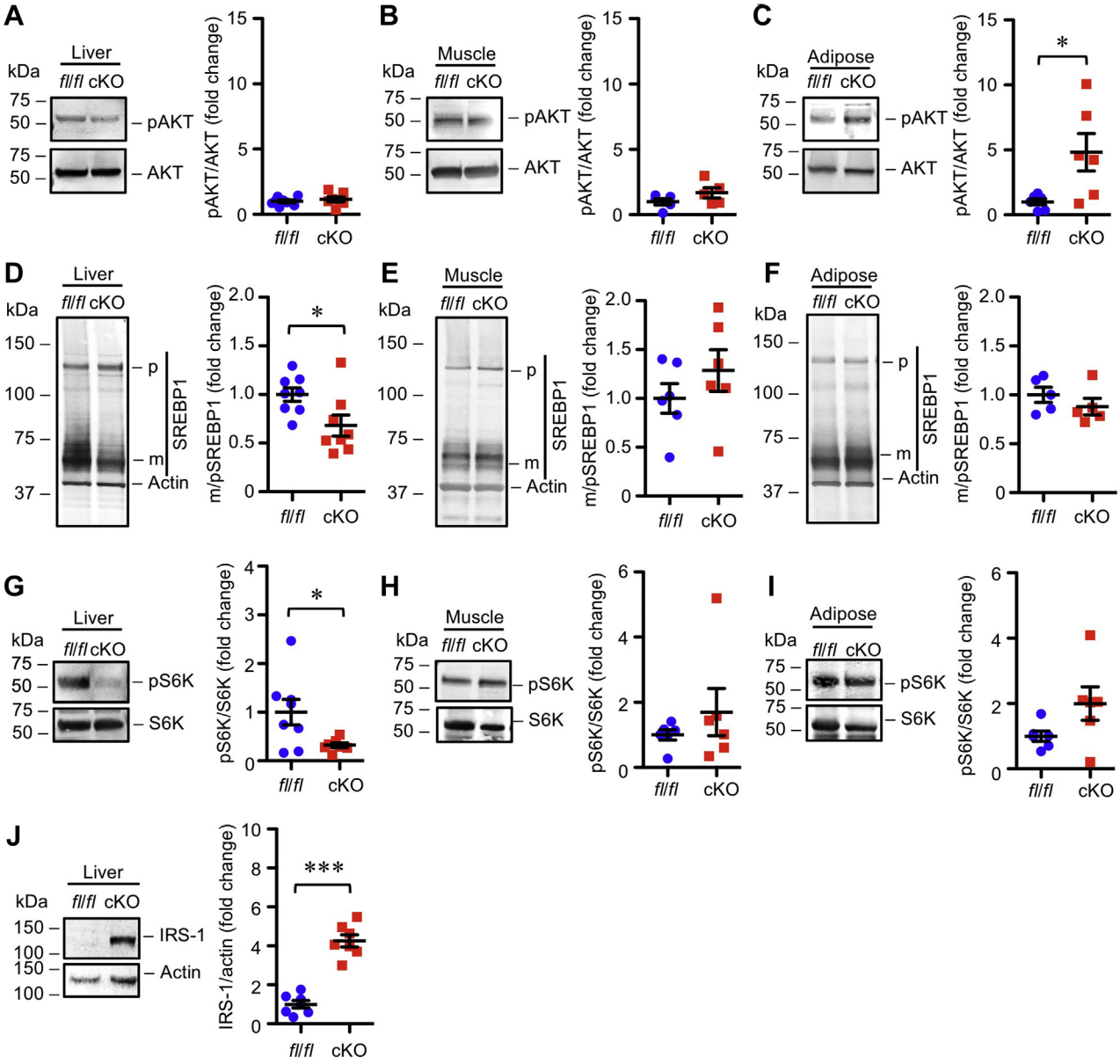

Figure 5. Systemic AKT/SREBP signaling in HFD-fed *Capns1*-targeted mice. Mice were fed an HFD for 18 weeks. *A*, protein expression of AKT in liver in HFD-fed mice (*fl/fl*: n = 8; cKO: n = 7). *B*, protein expression of AKT in skeletal muscle in HFD-fed mice (*fl/fl*: n = 5; cKO: n = 5). *C*, protein expression of AKT in adipose tissue in HFD-fed mice (*fl/fl*: n = 6; cKO: n = 6). *D*, protein expression of SREBP1 in liver in HFD-fed mice (*fl/fl*: n = 8; cKO: n = 8). *E*, protein expression of SREBP1 in skeletal muscle in HFD-fed mice (*fl/fl*: n = 6; cKO: n = 6). *F*, protein expression of SREBP1 in adipose tissue in HFD-fed mice (*fl/fl*: n = 5; cKO: n = 5). *G*, protein expression of P70 S6 kinase in liver in HFD-fed mice (*fl/f*: n = 8; cKO: n = 7). *H*, protein expression of P70 S6 kinase in skeletal muscle in HFD-fed mice (*fl/fl*: n = 6; cKO: n = 6). *I*, protein expression of P70 S6 kinase in adipose tissue in HFD-fed mice (*fl/fl*: n = 6; cKO: n = 6). *J*, protein expression of IRS-1 in liver in HFD-fed mice (*fl/fl*: n = 7; cKO: n = 7). Two-tailed Student's *t* test was used for the statistical analysis (*C–F*, *I*, and *J*). *$p < 0.05$. cKO, conditional KO; HFD, high-fat diet; IRS-1, insulin receptor substrate 1; SREBP, sterol regulatory element–binding protein.

Among AKT signaling molecules, the mTOR–S6K signaling axis is reportedly involved in the maturation of SREBP1 (29). Furthermore, the mTOR–S6K axis can be uncoupled from AKT signaling pathways, as S6K negatively controls insulin signaling *via* negative feedback of the insulin receptor substrate (IRS)–AKT axis (30, 31). These observations are consistent with our current data; therefore, S6K signaling was monitored in metabolic organs. Immunoblot analysis revealed that phosphorylation of S6K in the livers of obese mice was markedly reduced by *Capns1* cKO (Fig. 5*G*), whereas S6K phosphorylation was unchanged in skeletal muscle and adipose tissue (Fig. 5, *H* and *I*). It was reported that S6K downregulates IRS-1 under conditions of hyperglycemia (30, 32). Consistently, targeting EC/hematopoietic *Capns1* restored IRS-1 protein expression levels in liver (Fig. 5*J*).

The LAT1–4F2hc complex is a major transporter of BCAAs (33) and is ubiquitously expressed in many nonepithelial cells, including hepatocytes (34). We examined the effects of pharmacological LAT1 inhibition *in vivo* to assess the requirement of BCAA for calpain-mediated triglyceride accumulation in liver. Administration of the LAT1 inhibitor, JPH203, to HFD-fed *Capns1* $^{fl/fl}$ mice reduced the triglyceride content of the

liver (Fig. 6*A*) without altering plasma triglyceride (Fig. 6*B*) and amino acid levels (Fig. 6*C*). Targeting EC/hematopoietic *Capns1* did not further downregulate triglyceride levels in the liver (Fig. 6*A*).

Discussion

Our data clearly show that conventional calpains are associated with the production of free amino acids in cultured ECs. Gene targeting in mice revealed that certain amino acids in fatty liver are dependent on EC calpain systems. Since circulating amino acid levels were unaffected by targeting conventional calpains, these proteases may contribute to the local amino acid production in fatty liver. Cell-based experiments further suggested that EC-derived amino acids are responsible for the acceleration of the mTORC1–S6K axis and subsequent lipogenesis in the surrounding hepatocytes (Fig. 7). The behavior of the S6K–SREBP1c pathway was reproduced in calpain-targeted mice. To the best of our knowledge, this is the first study to report local amino acid production by calpain proteolytic systems.

Our findings showed that extracellular high glucose concentrations as well as Ca^{2+} ionophores facilitated the production of amino acids in cultured ECs in a calpain-dependent manner. High–molecular weight proteins in cultured ECs were preferentially degraded under high glucose conditions; thus, those calpain substrates may be a source of the extracellular amino acids. Since conventional calpains recognize diverse amino acid sequences (35), they are able to proteolyze a variety of substrates, including high–molecular weight cytoskeletal proteins and adhesion molecules (36). These proteases usually recognize one to several cleavage sites per target substrate and are unable to directly convert their substrates into amino acids. Accordingly, it was suspected that other proteolytic systems may be involved in calpain-mediated amino acid production. Our data suggest that Ca^{2+} influx potentiates the proteasomal activity in ECs, and the combination of calpain inhibitor with proteasomal inhibitor resulted in a substantial reduction in amino acid production in ECs. In contrast, amino acid production was not reduced by proteasomal inhibitor alone. Calpain-mediated ubiquitin/proteasomal regulation was not responsible for the amino acid production since calpain inhibition did not influence proteasomal activity and protein ubiquitination. Tomita *et al.* (20) reported that calpain-induced limited proteolytic cleavage is necessary for the proteasomal degradation of retinoblastoma proteins, which is a transcriptional modulator. This suggests that calpain-induced preprocessing of target proteins can sensitize proteasomal protein degradation. Therefore, it appears that the calpain systems induce limited proteolysis of substrate proteins, which exert amino acid production coordinated with the proteasomal systems.

Our cell-based experiments showed that calpain activity in cultured ECs was responsible for the production of most amino acid types. In contrast, animal experiments indicated that certain amino acid types, including leucine, isoleucine, and glycine, in the liver microenvironment were dependent on EC calpain systems. This indicates that EC calpain substantially contributes to the amounts of these three amino acid types in the liver compared with their physiological levels. Leucine potentiates protein synthesis–related elements, including mTORC1 (37). The combination of leucine with other amino acids, including glycine, facilitates S6K phosphorylation, whereas glycine alone has no effect on the mTORC1–S6K axis (38). This is consistent with our data that indicated that targeted knockdown of the calpain systems in ECs accelerates leucine enrichment in the microenvironmental amino acid pool in the liver and that leucine supplementation in HepG2 cells exclusively upregulates insulin-induced S6K phosphorylation. Furthermore, conditioned media derived

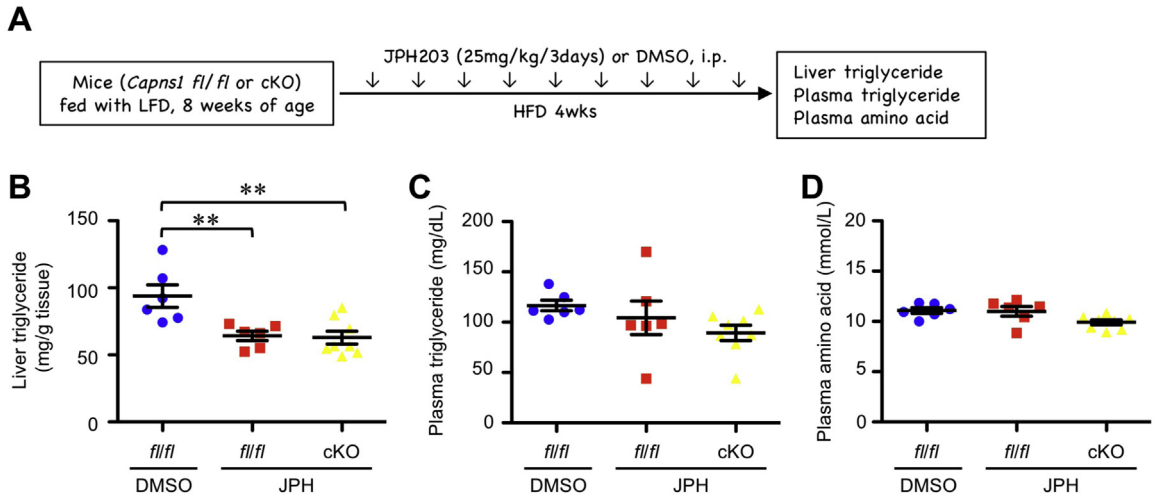

Figure 6. Effects of intervention of amino acid transporter on calpain-mediated triglyceride accumulation in liver. *In vivo* effects of amino acid transporter inhibitor JPH203 on hepatic triglyceride accumulation in HFD-fed mice. *A*, schematic overview of the pharmacological study. Control vehicle (dimethyl sulfoxide [DMSO]) or JPH203 (30 mg/kg) was intraperitoneally administered to HFD-fed mice for 4 weeks at an interval of 2 days. *B*, triglyceride levels in liver (*fl/fl* + DMSO: n = 6; *fl/fl* + JPH: n = 6; cKO + JPH: n = 8). *C*, triglyceride levels in plasma (*fl/fl* + DMSO: n = 6; *fl/fl* + JPH: n = 6; cKO + JPH: n = 8). *D*, amino acid levels in plasma (*fl/fl* + DMSO: n = 6; *fl/fl* + JPH: n = 6; cKO + JPH: n = 8). Statistical analysis was performed using one-way ANOVA with Bonferroni post hoc test (*B*). $^{**}p < 0.01$. cKO, conditional KO; HFD, high-fat diet.

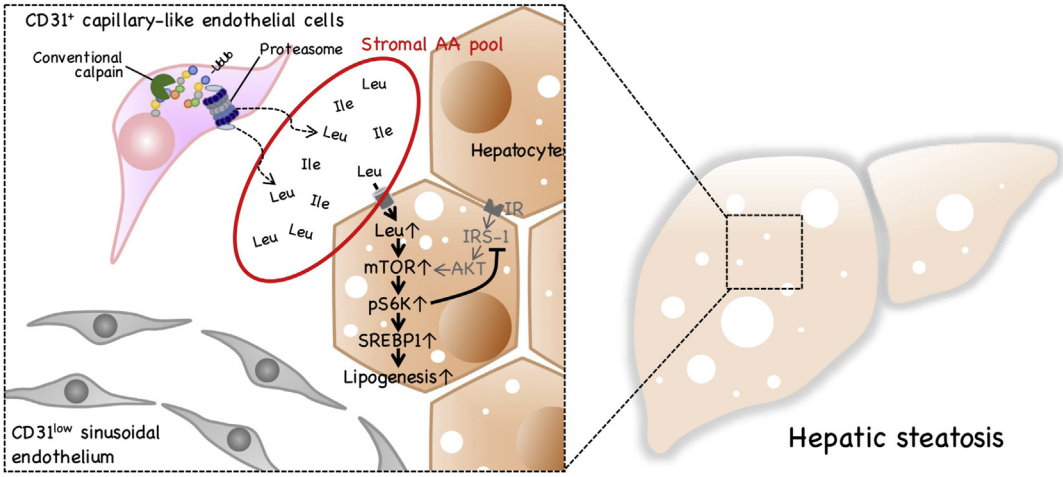

Figure 7. Schematic illustration of calpain-induced amino acid production in ECs in fatty liver. Calpain proteolytic systems, which are potentiated in CD31^{+}-capillary-like ECs in fatty liver, promoted amino acid production in the cells by coordinating with proteasomes. Calpain-generated environmental amino acids induced *de novo* lipogenesis in adjacent hepatocytes *via* the S6K–SREBP1 axis independent of AKT signaling. Consistently, targeting calpain systems specifically in ECs can reduce levels of environmental amino acids, including leucine, isoleucine, and glycine, in liver and can mitigate HFD-induced hepatic steatosis without altering plasma lipid or amino acid composition. EC, endothelial cell; S6K, S6 kinase; SREBP1, sterol regulatory element–binding protein 1.

from EC culture potentiated S6K phosphorylation and subsequent *de novo* lipogenesis in HepG2 cells, which was reversed by LAT1 inhibition. Consistent with this, it was reported that pharmacological inhibition of LAT1 reduced leucine incorporation in isolated pancreatic islets (39). Collectively, lipogenesis in hepatocytes may be strongly upregulated when EC-derived amino acids, particularly leucine, accumulate in the cells.

The present study showed that EC/hematopoietic cell–specific targeting of calpain systems upregulated mSREBP1c and its expression levels in liver, whereas AKT and FOXO1 phosphorylation remained unchanged. Hence, calpain systems in ECs facilitate the control of SREBP1c to facilitate lipogenesis in hepatocytes, independent of AKT-mediated pathways. While the insulin–AKT signaling axis is reportedly transduced *via* IRS-1 under the physiological status, this adaptive protein appears to be downregulated under hyperglycemic conditions (31). Therefore, insulin signaling is uncoupled from metabolic signaling, including glyconeogenesis and lipogenesis, leading to insulin resistance. S6K phosphorylates IRS-1 and IRS-2 to degrade these adaptive proteins (30, 32), suggesting that overactivation of S6K and its feedback interference of IRS may be a cause of uncoupling. Importantly, the mTORC1–S6K axis can be activated by environmental factors, such as amino acids, as well as inflammatory cytokines and high glucose concentrations in an AKT-independent manner, which may direct the processing of SREBP1c and *de novo* lipogenesis (29). Consistently, transduction of the amino acid transporter SNAT2 specifically to the liver upregulates S6K, thereby inducing steatohepatitis (8), suggesting that excessive accumulation of amino acids in hepatocytes may be a cause of hepatic steatosis *via* S6K. Our data revealed that conditional targeting of conventional calpains recovered the IRS-1 expression levels even under hyperglycemic conditions. Since AKT phosphorylation in liver was not reversed in mice with targeted abolition of conventional calpains, IRS-1 upregulation alone may not be sufficient to normalize the hyperglycemic uncoupling of AKT signaling. These results suggest that both EC/hematopoietic cell–specific targeting of calpain and LAT1 inhibition ameliorated HFD-induced fatty liver independently of plasma triglyceride and amino acid levels. Importantly, targeted abolition of calpain systems did not further downregulate hepatic triglyceride levels in mice treated with an LAT1 inhibitor, indicating that calpain-generated environmental amino acids are involved in the AKT-independent lipogenesis in fatty liver. Hematopoietic calpain was not found to be involved in lipid handling; therefore, it is reasonable to suggest that calpain systems in ECs have a substantial impact on the mTORC1–S6K–SREBP1c axis in hepatocytes.

In addition to hepatic steatosis, EC/hematopoietic calpain knockdown improved insulin sensitivity in HFD-fed mice. Conditional targeting of calpain systems did not upregulate AKT phosphorylation in liver; thus, AKT signaling in the liver may not contribute to insulin sensitization. Alternatively, AKT phosphorylation and FOXO1 downregulation were detected in adipose tissue in response to calpain knockdown. Conditional targeting of calpain systems did not significantly modify glucose tolerance and systemic insulin homeostasis; thus, we concluded that EC calpain in adipose tissue is mainly associated with insulin sensitization *via* unknown mechanisms. Further studies are required to elucidate the causal relationship between AKT regulation by EC calpain systems and insulin sensitization.

The findings of the present study clarify the proteolytic production of amino acids in the liver microenvironment *via* intracellular proteolytic systems in ECs and indicate that calpain-induced amino acid production may be a cause of hepatic steatosis. Since proteolytic amino acid production occurs independent of systemic homeostasis, normalization of the amino acid pool in the liver microenvironment represents a novel approach to mediate steatotic susceptibility in the liver. Conventional EC calpains are reportedly activated in

atherosclerosis (19), cancer, and retinopathy (15), and understanding calpain-induced amino acid production in these diseases is of interest.

Experimental procedures

Animals

All mice (C57BL/6J background) were housed in climate-controlled (21 °C) specific pathogen-free facilities with a 12 h light–dark cycle and free access to standard laboratory food (Picolab mouse diet 20; Laboratory Diet) and water. Diet-induced obesity experiments were performed in 8-week-old female mice housed in wire cages and fed an LFD (CRF-1; Oriental Yeast Co) or HFD (F2HFD1; CRF-1 supplemented with 16.5% fat, 1.25% cholesterol, and 0.5% sodium cholate; Oriental Yeast Co) for 18 weeks. LNL–*CAST* Tg (15) and *Capns1* $^{fl/fl}$ (40) mice were generated as previously described. EC/hematopoietic cell–specific *Capns1* cKO mice were generated by intercrossing *Capns1* $^{fl/fl}$ mice with Tie2–Cre Tg mice (Jackson Laboratory; stock no.: 008863) (41), with *Capns1* $^{fl/fl}$ mice used as controls. EC/hematopoietic cell–specific *CAST* cTg mice were generated by intercrossing LNL–*CAST* Tg with Tie2–Cre Tg mice, with LNL–*CAST* Tg mice used as controls. Genotypes were confirmed using standard PCR-based genotyping (Table S1). All samples were obtained from animals following euthanasia *via* isoflurane overdose at the end point. Animals whose condition exceeded the humane end point set by ethical approval were excluded prior to the experimental end point. All experimental procedures were approved by the Institutional Animal Care and Use Committee of Showa University (ref. 09071,02067,03084) and the Institutional Biosafety Committee of Showa University (ref. 1806,2005) and were conducted in accordance with the guidelines of the National Institutes of Health (NIH) Guide for the Care and Use of Laboratory Animals of the Animal Care and Use Committee Guideline of Showa University.

Bone marrow transplantation

Bone marrow transplantation was performed as previously described (42, 43). Briefly, recipient wildtype mice were irradiated with 8 Gy of X-rays for 10 min and intravenously injected with bone marrow cells (1×10^7 cells per animal) derived from *Capns1* $^{fl/fl}$ or *Capns1* cKO donor mice and suspended in Hank's balanced salt saline (HBSS). Four weeks after injection, the animals were fed an HFD for 18 weeks. Successful chimerism was confirmed using PCR-based genotyping of bone marrow cells.

Isolation of hepatic EC fraction and isolation of bone marrow–derived macrophages

LFD- or HFD-fed mice were anesthetized *via* inhalation of isoflurane, and their circulatory systems were perfused using PBS through the left ventricle. Samples of liver (750–1200 mg) were minced and briefly dissociated using a gentleMACS Dissociator (Miltenyi Biotec) with the m_liver_01.02 program. The dissociated samples were then digested in Krebs–Ringer buffer (154 mmol/l NaCl, 5.6 mmol/l KCl, 10 mmol/l $CaCl_2$, 2 mmol/l $MgCl_2$, 5.5 mmol/l glucose, 20.1 mmol/l Hepes, 25 mmol/l $NaHCO_3$; pH 7.4) containing 500 CDU/ml collagenase IV (Sigma–Aldrich) and 150 U/ml DNase I (Applichem) at 37 °C for 30 min and then further dissociated using a gentleMACS Dissociator with the m_liver_02.02 program. The samples were then filtered using a 100 μm cell strainer and supplemented with 10 ml of PBS containing 0.5% bovine serum albumin (BSA) and 2 mmol/l EDTA. The filtered cell suspension was centrifuged at 20*g* for 4 min at 4 °C to remove the pelleted hepatocytes. The EC-containing supernatant was centrifuged at 300*g* for 10 min at 4 °C, and the pellet was lysed with red blood cell lysis buffer (BD Pharm Lyse; BD Pharmingen) to remove the erythrocytes. The EC-containing cell fraction was seeded onto culture vessels and cultured in Dulbecco's modified Eagle's medium (DMEM) containing 10% fetal bovine serum (FBS) for 10 min. Unbound cells were removed by washing with medium, and attached cells served as hepatic ECs. Bone marrow–derived macrophages were prepared by collecting murine bone marrow cells by shearing femoral bone marrows with culture medium and incubating the cells in RPMI1640 (Sigma) supplemented with 10% FBS, penicillin–streptomycin–amphotericin B (Wako Pure Chemicals) and macrophage colony-stimulating factor (50 ng/ml) to stimulate differentiation to macrophages. After 5 days of culture, unbound cells were removed by washing with medium, and differentiated macrophages were then stimulated with high glucose concentrations (25 mmol/l).

Glucose and insulin tolerance tests

Glucose tolerance was measured by fasting mice for 16 h followed by i.p. injection with 1 g/kg glucose. Insulin tolerance was measured by fasting mice for 4 to 6 h followed by i.p. injection with 0.5 U/kg insulin. Blood was then collected from the tail vein *via* at 15, 30, 60, and 120 min after injection. Blood glucose levels were measured using a Glutest I (SKK) equipped with a sensor.

Administration of JPH203

In vivo assessment of JPH203 was performed as previously described (44). Control vehicle (dimethyl sulfoxide) or JPH203 (MCE; 30 mg/kg) was dissolved in isotonic saline and intraperitoneally administered to HFD-fed mice for 4 weeks from 8 weeks of age at 2-day intervals.

Histology

Tissues were fixed with 4% paraformaldehyde, embedded into optimal cutting temperature compound (Sakura Finetek), and cryosectioned at a thickness of 5 μm. For immunohistochemistry analysis, antigen retrieval was performed using HistoVT One (Nacalai Tesque) at 70 °C for 20 min. Specimens were blocked with 5% BSA and then incubated with the appropriate primary antibodies (Table S2) dissolved in PBS containing 1% BSA. Specimens were then labeled with an appropriate fluorescent secondary antibody. Oil Red O staining was performed to determine lipid accumulation in liver tissues. Sirius red staining (Picro Sirius Red; ScyTek) was

performed to evaluate hepatic fibrosis. Images were acquired using a fluorescent microscope (Nikon) and analyzed using ImageJ software (NIH).

Measurement of liver triglyceride levels

Triglyceride-enriched lipids in the liver were extracted using the procedure previously described by Folch *et al.* (45). A piece of liver tissue (approximately 50 mg wet weight) was homogenized in 500 μl of 2:1 chloroform/methanol solution. Undissolved protein precipitates were removed by centrifugation at 2000 rpm for 5 min. The samples were then supplemented with 0.2 volume of water and centrifuged at 2000 rpm for 5 min to separate the upper methanol layer from the lower chloroform layer. The chloroform layer was then isolated and evaporated to obtain the lipid-containing residues. The residue was dissolved in 50 μl of 3:2 hexane/isopropanol. Triglyceride levels of the samples were determined using Lab Assay Triglyceride kits (Wako) and a VersaMAX microplate reader (Molecular Devices), and the values were normalized to the wet weights of the dissected liver samples.

Amino acid and BCAA measurements

The amount of amino acid in the culture supernatant was quantified using liquid chromatography–tandem mass spectrometry. Briefly, a triple quadrupole mass spectrometer equipped with an electrospray ionization ion source (LCMS-8060; Shimadzu Corporation) was used in the positive electrospray ionization and multiple reaction monitoring modes. The samples were resolved on the Discovery HS F5-3 column (2.1 mm I.D. × 150 mm/l, 3 μm particle; Sigma–Aldrich), using a step gradient with mobile phase A (0.1% formate) and mobile phase B (0.1% acetonitrile) at ratios of 100:0 (0–5 min), 75:25 (5–11 min), 65:35 (11–15 min), 5:95 (15–20 min), and 100:0 (20–25 min) at a flow rate of 0.25 ml/min and column temperature of 40 °C. Quantification of amino acids was performed by monitoring the ion transitions as previously described (46). Amino acids were measured in liver samples using a piece of liver tissue (approximately 50 mg wet weight) homogenized in 150 μl of PBS on ice. The samples were then centrifuged at 15,000*g* to remove undissolved debris and hepatocytes. The supernatants served as liver microenvironmental samples. Total L-amino acids in the samples were quantified using the L-Amino Acid Quantitation Kit (Sigma–Aldrich) and normalized to their protein concentrations. Similarly, BCAAs were measured in the samples using a BCAA assay kit (Cell Biolabs, Inc). Individual amino acids were quantified in liver samples by analyzing the liver extracts by HPLC as previously described (47, 48). Liver tissues were homogenized in 500 μl of 0.2 mol/l perchloric acid and left to deproteinize on ice for 30 min. The samples were then centrifuged at 20,000*g* to remove undissolved debris. Supernatants were purified using 0.2 μm of hydrophilic polytetrafluoroethylene filters. The amino acids in the samples were quantified using a Waters HPLC system (Pico-Tag free amino acid analysis column [3.9 mm × 300 mm], Alliance e2695 separation module, 2487 dual-wavelength UV detector, and Empower software; Waters). Intracellular BCAA levels were measured by stimulating cultured ECs with 5 μmol/l ionomycin. The cells were then harvested and lysed in a lysis buffer, and BCAAs were measured in lysed cells using a BCAA assay kit (Cell Biolabs). The total amino acid content was measured in the culture supernatant by stimulating cultured ECs with 5 μmol/l ionomycin in the presence or the absence of calpaptin or bortezomib for 30 min and quantifying the amino acid levels of the culture supernatants using an amino acid measurement kit (Sigma–Aldrich).

Plasma insulin

Plasma insulin levels were measured in *Capns1*$^{fl/fl}$ and cKO mice using Mouse Insulin ELISA kit (Morinaga Institute of Biological Science, Inc) according to the manufacturer's instructions. Samples were acquired from tail veins *via* venous bleeding from mice fasted for 16 h. Plasma samples were also obtained from the mice 2 h after refeeding.

Plasma lipid profiling

Blood samples were acquired from the tail veins of mice fasted for 16 h and then refed for 2 h. Lipoprotein-based plasma lipid profiles were evaluated by HPLC-based LipoSEARCH (Skylight Biotech, Inc) analysis.

HepG2 culture and amino acid evaluation

The HepG2 hepatocyte cell line was obtained from the National Institute of Biomedical Innovation (Tsukuba). The cells were cultured in low glucose DMEM (Wako) supplemented with 1% (v/v) penicillin–streptomycin and 10% (v/v) FBS and maintained in 5% CO_2 at 37 °C under humidified conditions. Individual amino acids were evaluated in confluent HepG2 cells harvested and seeded onto a 12-well plate at a density of 5×10^5 cells per well. Culture medium was replaced 24 h after subculture with HBSS (1.26 mmol/l $CaCl_2$, 0.49 mmol/l $MgCl_2$, 0.41 mmol/l $MgSO_4$, 5.33 mmol/l KCl, 0.44 mmol/l KH_2PO_4, 4.17 mmol/l $NaHCO_3$, 138 mmol/L NaCl, 0.34 mmol/l Na_2HPO_4, 5.56 mmol/l D-glucose; pH 7.4) supplemented with leucine, isoleucine, or valine. After 16 h, cells were stimulated with 100 nmol/l insulin for 15 min and lysed for immunoblot analysis.

EC culture and conditioned media experiments

HUVECs were purchased from Takara Bio, Inc. The cells were cultured in endothelial growth medium (Takara Bio) and maintained in 5% CO_2 at 37 °C under humidified conditions. The murine EC MS1 cell line was purchased from American Type Culture Collection and cultured in DMEM supplemented with 10% FBS and antibiotics. Cells were exposed to high glucose concentrations by replacing the EC culture medium of culture with Krebs–Ringer buffer containing glucose at 25 mmol/l. Krebs–Ringer buffer containing 5.5 mmol/l glucose was used for low glucose concentrations. Inhibitor experiments were performed by pretreating HUVECs with

10 μmol/l calpeptin or 10 μmol/l bortezomib for 30 min followed by treatment with ionomycin in the presence of the inhibitor. Conditioned media were acquired by stimulating HUVECs with 5 μmol/l ionomycin for 5 min in Ca^{2+}-deprived HBSS. The Ca^{2+}-deprived HBSS was then replaced with Ca^{2+}-containing HBSS without ionomycin, and the cells were incubated for 30 min in 5% CO_2 at 37 °C under humidified conditions to allow Ca^{2+} influx into the HUVECs in the absence of ionomycin. The culture supernatant was harvested as the conditioned medium. HepG2 cells were seeded into a 12-well plate at a density of 5×10^5 cells per well. At 24 h after subculture, the medium was replaced with the conditioned media derived from ionomycin-stimulated or control HUVEC cultures, and the HepG2 cells were incubated for 16 h. The cells were then stimulated with 100 nmol/l insulin for 15 min and lysed for immunoblot analysis. Pharmacological inhibitors of 10 nmol/l rapamycin (Cayman Chemical) or 50 nmol/l JPH203 (MCE) were added as required to the HepG2 culture 30 min prior to insulin treatment.

Luminometric assessment of calpain and proteasomal activity

Luminescent calpain activity and proteasomal activity were measured using the Calpain-Glo Assay Kit (Promega) and Proteasome-Glo Assay Kit (chymotrypsin-like; Promega), respectively, according to the manufacturer's instructions. HUVECs were stimulated with 5 μmol/l ionomycin for 30 min and then lysed with 0.9% Triton X-100. Cell debris was removed by centrifugation at 15,000 rpm, and then 75 μl of cell lysate was mixed with an equal volume of Calpain-Glo Reagent or Proteasome-Glo Reagent and incubated for 10 min. Luminescence was then measured by using a Mithoras LB940 luminescence plate reader (Berthold Technologies) as an index of their activity.

Lipogenesis in cultured cells

De novo lipogenesis was measured by incubating HepG2 cells in DMEM (Wako) containing 100 nmol/l insulin, 0.05 mg/ml palmitic acid (Sigma–Aldrich), and 1% (w/v) BSA for 24 h. Cells were then fixed with PBS containing 4% paraformaldehyde for 30 min at 4 °C. The cells were washed three times with PBS and then incubated for 30 min in the dark with 1 μmol/l LipiDye (Lipid Droplet Green; Funakoshi), which specifically reacts with neutral lipids, such as triglycerides (49), and counterstained with 4′,6-diamidino-2-phenylindole. Images were acquired using a fluorescence microscope (IX-83; Olympus). The images were analyzed using ImageJ software (NIH).

Transfection with siRNAs

HUVECs were transfected with either 40 nmol/l stealth siRNAs against CAPNS1 or 40 nmol/l nonsilencing control RNA (GC medium; Ambion) using siPORT NeoFX Transfection Agent (Ambion) according to the manufacturer's instructions. HUVECs were used for experiments 48 h after transfection. Details of the siRNAs are shown in Table S3.

qRT–PCR

qRT–PCR was performed as described previously (14, 15, 19). Total RNA was isolated from liver by homogenizing a piece of liver (approximately 50 mg in wet weight) in 1 ml TRIzol reagent (Ambion). Total RNA (3 μg per reaction) was converted into complementary DNA using Revertra Ace (Toyobo). qRT–PCR was performed using Power SYBR Green Master Mix (Thermo Fisher Scientific, Inc) and a 7900HT Real-Time PCR System (Applied Biosystems). The sequences of the primers used for qPCR are listed in Table S4.

Immunoblot analysis

Mouse tissues or cultured cells were lysed using lysis buffer (125 mmol/l NaCl, 20 mmol/l Tris–HCl, 0.1% SDS, 1% Triton X-100, 1% sodium deoxycholate; pH 7.4) followed by centrifugation at 15,000 rpm for 5 min at 4 °C to remove undissolved debris. The lysates were then sonicated (Handy Sonic UR-20 P; Tomy Seiko Co, Ltd) on ice. Protein concentrations of the lysates were quantified using the Pierce BCA Protein Assay Kit (Thermo Fisher Scientific). Equal amounts of protein were loaded onto SDS–PAGE gels, transferred to polyvinylidene difluoride membranes (Wako), and incubated overnight with the primary antibody of interest. Alkaline phosphatase–conjugated secondary antibody (Cell Signaling) and 5-bromo-4-chloro-3-indolyl-phosphate–nitro blue tetrazolium (Wako) were used to detect the target proteins. The primary antibodies used for immunoblotting are listed in Table S2. Coomassie brilliant blue staining was conducted using Rapid CBB KANTO (KANTO Chemical Co) according to the manufacturer's instructions.

Statistical analysis

Data are expressed as mean ± SEM. Statistical comparisons were made using either one-way or two-way ANOVA followed by Bonferroni's post hoc analysis. The significance of differences between two groups was determined using Student's unpaired two-tailed t test. Statistical significance was set at $p < 0.05$. All analyses were performed using GraphPad Prism, version 5.0 (GraphPad Software, Inc).

Data availability

All data generated and analyzed during this study are available from the corresponding author on reasonable request.

Supporting information—This article contains supporting information.

Acknowledgments—We thank Enago (www.enago.co.jp) for the English language review.

Author contributions—T. M. conceptualization; R. A., T. M., M. Z. E., Y. S., Y. T., S. H., V. S. C methodology; R. A. and T. M. formal analysis; R. A., T. M., M. Z. E., Y. S., Y. T., S. H., and V. S. C. investigation; K. O. resources; R. A. and T. M. writing–original

draft; T. M. and A. M. writing–review & editing; R. A. and T. M. visualization; A. M. supervision; T. M. project administration; T. M. and A. M. funding acquisition.

Funding and additional information—This study was supported in part by the Japan Society for the Promotion of Science KAKENHI grant (grant nos.: JP21K08585 [to A. M.], JP19K08590 [to T. M.], JP22H03520 [to T. M.], and JP19H03110 [to V. S. C.]), research grant from Bristol-Myers Squibb (to T. M.), personal chair grant from the British Heart Foundation (grant nos.: CH/11/3/29051 and RG/16/15/32294 [to K. O.]), research grant from the Suzuken Memorial Foundation (to T. M.), and research grant from the Mochida Memorial Foundation for Medical and Pharmaceutical Research (to T. M.), and a research grant from the Naito Memorial Foundation (to T. M.).

Conflict of interest—The authors declare that they have no conflicts of interest with the contents of this article.

Abbreviations—The abbreviations used are: BCAA, branched-chain amino acid; BSA, bovine serum albumin; cKO, conditional KO; cTg, conditional transgenic; DMEM, Dulbecco's modified Eagle's medium; EC, endothelial cell; FBS, fetal bovine serum; HBSS, Hank's balanced salt saline; HFD, high-fat diet; HUVEC, human umbilical vein endothelial cell; IRS, insulin receptor substrate; LAT1, L-type amino acid transporter 1; LFD, low-fat diet; mSREBP1, mature form of SREBP1; mTORC1, mammalian target of rapamycin complex 1; NIH, National Institutes of Health; qRT–PCR, quantitative real-time PCR; S6K, S6 kinase; SREBP1, sterol regulatory element–binding protein 1; VE, vascular endothelial.

References

1. Chalasani, N., Younossi, Z., Lavine, J. E., Diehl, A. M., Brunt, E. M., Cusi, K., Charlton, M., and Sanyal, A. J. (2012) The diagnosis and management of non-alcoholic fatty liver disease: Practice guideline by the American gastroenterological association, American association for the study of liver diseases, and American college of gastroenterology. *Gastroenterology* **142**, 1592–1609
2. Anderson, N., and Borlak, J. (2008) Molecular mechanisms and therapeutic targets in steatosis and steatohepatitis. *Pharmacol. Rev.* **60**, 311–357
3. Lynch, C. J., and Adams, S. H. (2014) Branched-chain amino acids in metabolic signalling and insulin resistance. *Nat. Rev. Endocrinol.* **10**, 723–736
4. White, P. J., and Newgard, C. B. (2019) Branched-chain amino acids in disease. *Science* **363**, 582–583
5. Le Couteur, D. G., Solon-Biet, S. M., Cogger, V. C., Ribeiro, R., de Cabo, R., Raubenheimer, D., Cooney, G. J., and Simpson, S. J. (2020) Branched chain amino acids, aging and age-related health. *Ageing Res. Rev.* **64**, 101198
6. Newgard, C. B. (2017) Metabolomics and metabolic diseases: Where do we stand? *Cell Metab.* **25**, 43–56
7. Fiehn, O., Garvey, W. T., Newman, J. W., Lok, K. H., Hoppel, C. L., and Adams, S. H. (2010) Plasma metabolomic profiles reflective of glucose homeostasis in non-diabetic and type 2 diabetic obese African-American women. *PLoS One* **5**, e15234
8. Uno, K., Yamada, T., Ishigaki, Y., Imai, J., Hasegawa, Y., Sawada, S., Kaneko, K., Ono, H., Asano, T., Oka, Y., and Katagiri, H. (2015) A hepatic amino acid/mTOR/S6K-dependent signalling pathway modulates systemic lipid metabolism via neuronal signals. *Nat. Commun.* **6**, 7940
9. Onodera, J., and Ohsumi, Y. (2005) Autophagy is required for maintenance of amino acid levels and protein synthesis under nitrogen starvation. *J. Biol. Chem.* **280**, 31582–31586
10. Suraweera, A., Münch, C., Hanssum, A., and Bertolotti, A. (2012) Failure of amino acid homeostasis causes cell death following proteasome inhibition. *Mol. Cell* **48**, 242–253
11. Miyazaki, T., Akasu, R., and Miyazaki, A. (2020) Calpain proteolytic systems counteract endothelial cell adaptation to inflammatory environments. *Inflamm. Regen.* **40**, 5
12. Miyazaki, T., and Miyazaki, A. (2018) Dysregulation of calpain proteolytic systems underlies degenerative vascular disorders. *J. Atheroscler. Thromb.* **25**, 1–15
13. Miyazaki, T., and Miyazaki, A. (2017) Defective protein catabolism in atherosclerotic vascular inflammation. *Front. Cardiovasc. Med.* **4**, 79
14. Miyazaki, T., Haraguchi, S., Kim-Kaneyama, J. R., and Miyazaki, A. (2019) Endothelial calpain systems orchestrate myofibroblast differentiation during wound healing. *FASEB J.* **33**, 2037–2046
15. Miyazaki, T., Taketomi, Y., Saito, Y., Hosono, T., Lei, X. F., Kim-Kaneyama, J. R., Arata, S., Takahashi, H., Murakami, M., and Miyazaki, A. (2015) Calpastatin counteracts pathological angiogenesis by inhibiting suppressor of cytokine signaling 3 degradation in vascular endothelial cells. *Circ. Res.* **116**, 1170–1181
16. Scalia, R., Gong, Y., Berzins, B., Zhao, L. J., and Sharma, K. (2007) Hyperglycemia is a major determinant of albumin permeability in diabetic microcirculation: The role of mu-calpain. *Diabetes* **56**, 1842–1849
17. Miyazaki, T., Koya, T., Kigawa, Y., Oguchi, T., Lei, X. F., Kim-Kaneyama, J. R., and Miyazaki, A. (2013) Calpain and atherosclerosis. *J. Atheroscler. Thromb.* **20**, 228–237
18. Goll, D. E., Thompson, V. F., Li, H., Wei, W., and Cong, J. (2003) The calpain system. *Physiol. Rev.* **83**, 731–801
19. Miyazaki, T., Taketomi, Y., Takimoto, M., Lei, X. F., Arita, S., Kim-Kaneyama, J. R., Arata, S., Ohata, H., Ota, H., Murakami, M., and Miyazaki, A. (2011) m-Calpain induction in vascular endothelial cells on human and mouse atheromas and its roles in VE-cadherin disorganization and atherosclerosis. *Circulation* **124**, 2522–2532
20. Tomita, T., Huibregtse, J. M., and Matouschek, A. (2020) A masked initiation region in retinoblastoma protein regulates its proteasomal degradation. *Nat. Commun.* **11**, 2019
21. Chen, H., Polo, S., Di Fiore, P. P., and De Camilli, P. V. (2003) Rapid Ca2+-dependent decrease of protein ubiquitination at synapses. *Proc. Natl. Acad. Sci. U. S. A.* **100**, 14908–14913
22. Wempe, M. F., Rice, P. J., Lightner, J. W., Jutabha, P., Hayashi, M., Anzai, N., Wakui, S., Kusuhara, H., Sugiyama, Y., and Endou, H. (2012) Metabolism and pharmacokinetic studies of JPH203, an L-amino acid transporter 1 (LAT1) selective compound. *Drug Metab. Pharmacokinet.* **27**, 155–161
23. Faivre, S., Kroemer, G., and Raymond, E. (2006) Current development of mTOR inhibitors as anticancer agents. *Nat. Rev. Drug Discov.* **5**, 671–688
24. Marcu, R., Choi, Y., Xue, J., Fortin, C., Wang, Y., Nagao, R., Xu, J., MacDonald, J., Bammler, T., Murry, C., Muczynski, K., Stevens, K., Himmelfarb, J., Schwartz, S., and Zheng, Y. (2018) Human organ-specific endothelial cell heterogeneity. *iScience* **4**, 20–35
25. Miyao, M., Kotani, H., Ishida, T., Kawai, C., Manabe, S., Abiru, H., and Tamaki, K. (2015) Pivotal role of liver sinusoidal endothelial cells in NAFLD/NASH progression. *Lab. Invest.* **95**, 1130–1144
26. Hamaguchi, I., Huang, X. L., Takakura, N., Tada, J., Yamaguchi, Y., Kodama, H., and Suda, T. (1999) *In vitro* hematopoietic and endothelial cell development from cells expressing TEK receptor in murine aorta-gonad-mesonephros region. *Blood* **93**, 1549–1556
27. Constien, R., Forde, A., Liliensiek, B., Gröne, H. J., Nawroth, P., Hämmerling, G., and Arnold, B. (2001) Characterization of a novel EGFP reporter mouse to monitor Cre recombination as demonstrated by a Tie2 Cre mouse line. *Genesis* **30**, 36–44
28. Shimano, H., and Sato, R. (2017) SREBP-regulated lipid metabolism: Convergent physiology - divergent pathophysiology. *Nat. Rev. Endocrinol.* **13**, 710–730
29. Yecies, J. L., Zhang, H. H., Menon, S., Liu, S., Yecies, D., Lipovsky, A. I., Gorgun, C., Kwiatkowski, D. J., Hotamisligil, G. S., Lee, C. H., and Manning, B. D. (2011) Akt stimulates hepatic SREBP1c and lipogenesis through parallel mTORC1-dependent and independent pathways. *Cell Metab.* **14**, 21–32

30. Patti, M. E., Brambilla, E., Luzi, L., Landaker, E. J., and Kahn, C. R. (1998) Bidirectional modulation of insulin action by amino acids. *J. Clin. Invest.* **101**, 1519–1529
31. Zhang, J., Gao, Z., Yin, J., Quon, M. J., and Ye, J. (2008) S6K directly phosphorylates IRS-1 on Ser-270 to promote insulin resistance in response to TNF-(alpha) signaling through IKK2. *J. Biol. Chem.* **283**, 35375–35382
32. Zhang, J., Gao, Z., Fau - Yin, J., Yin, J., Fau - Quon, M. J., Quon, Mj, Fau - Ye, J., and Ye, J. (2008) S6K directly phosphorylates IRS-1 on Ser-270 to promote insulin resistance in response to TNF-(alpha) signaling through IKK2. *J. Biol. Chem.* **283**, 35375–35382
33. Verrey, F. (2003) System L: Heteromeric exchangers of large, neutral amino acids involved in directional transport. *Pflugers Arch.* **445**, 529–533
34. Javed, K., and Fairweather, S. J. (2019) Amino acid transporters in the regulation of insulin secretion and signalling. *Biochem. Soc. Trans.* **47**, 571–590
35. Shinkai-Ouchi, F., Koyama, S., Ono, Y., Hata, S., Ojima, K., Shindo, M., duVerle, D., Ueno, M., Kitamura, F., Doi, N., Takigawa, I., Mamitsuka, H., and Sorimachi, H. (2016) Predictions of cleavability of calpain proteolysis by quantitative structure-activity relationship analysis using newly determined cleavage sites and catalytic efficiencies of an oligopeptide array. *Mol. Cell Proteomics* **15**, 1262–1280
36. Miyazaki, T., Honda, K., and Ohata, H. (2007) Requirement of Ca2+ influx- and phosphatidylinositol 3-kinase-mediated m-calpain activity for shear stress-induced endothelial cell polarity. *Am. J. Physiol. Cell Physiol.* **293**, C1216–C1225
37. Son, S. M., Park, S. J., Lee, H., Siddiqi, F., Lee, J. E., Menzies, F. M., and Rubinsztein, D. C. (2019) Leucine signals to mTORC1 *via* its metabolite acetyl-coenzyme A. *Cell Metab.* **29**, 192–201.e7
38. Dyachok, J., Earnest, S., Iturraran, E. N., Cobb, M. H., and Ross, E. M. (2016) Amino acids regulate mTORC1 by an obligate two-step mechanism. *J. Biol. Chem.* **291**, 22414–22426
39. Cheng, Q., Beltran, V. D., Chan, S. M., Brown, J. R., Bevington, A., and Herbert, T. P. (2016) System-L amino acid transporters play a key role in pancreatic β-cell signalling and function. *J. Mol. Endocrinol.* **56**, 175–187
40. Taneike, M., Mizote, I., Morita, T., Watanabe, T., Hikoso, S., Yamaguchi, O., Takeda, T., Oka, T., Tamai, T., Oyabu, J., Murakawa, T., Nakayama, H., Nishida, K., Takeda, J., Mochizuki, N., *et al.* (2011) Calpain protects the heart from hemodynamic stress. *J. Biol. Chem.* **286**, 32170–32177
41. Kisanuki, Y. Y., Hammer, R. E., Miyazaki, J., Williams, S. C., Richardson, J. A., and Yanagisawa, M. (2001) Tie2-Cre transgenic mice: A new model for endothelial cell-lineage analysis *in vivo*. *Dev. Biol.* **230**, 230–242
42. Kigawa, Y., Miyazaki, T., Lei, X. F., Nakamachi, T., Oguchi, T., Kim-Kaneyama, J. R., Taniyama, M., Tsunawaki, S., Shioda, S., and Miyazaki, A. (2014) NADPH oxidase deficiency exacerbates angiotensin II-induced abdominal aortic aneurysms in mice. *Arterioscler Thromb. Vasc. Biol.* **34**, 2413–2420
43. Miyazaki, T., Tonami, K., Hata, S., Aiuchi, T., Ohnishi, K., Lei, X. F., Kim-Kaneyama, J. R., Takeya, M., Itabe, H., Sorimachi, H., Kurihara, H., and Miyazaki, A. (2016) Calpain-6 confers atherogenicity to macrophages by dysregulating pre-mRNA splicing. *J. Clin. Invest.* **126**, 3417–3432
44. Yothaisong, S., Dokduang, H., Anzai, N., Hayashi, K., Namwat, N., Yongvanit, P., Sangkhamanon, S., Jutabha, P., Endou, H., and Loilome, W. (2017) Inhibition of l-type amino acid transporter 1 activity as a new therapeutic target for cholangiocarcinoma treatment. *Tumor Biol.* https://doi.org/10.1177/1010428317694545
45. Folch, J., Lees, M., and Sloane Stanley, G. H. (1957) A simple method for the isolation and purification of total lipides from animal tissues. *J. Biol. Chem.* **226**, 497–509
46. Oka, M., Hashimoto, K., Yamaguchi, Y., Saitoh, S. I., Sugiura, Y., Motoi, Y., Honda, K., Kikko, Y., Ohata, S., Suematsu, M., Miura, M., Miyake, K., Katada, T., and Kontani, K. (2017) Arl8b is required for lysosomal degradation of maternal proteins in the visceral yolk sac endoderm of mouse embryos. *J. Cell Sci.* **130**, 3568–3577
47. Han, G., Ouchi, Y., Hirota, T., Haraguchi, S., Miyazaki, T., Arakawa, T., Masuhara, N., Mizunoya, W., Tatsumi, R., Tashiro, K., Bungo, T., Furuse, M., and Chowdhury, V. S. (2020) Effects of l-leucine in ovo feeding on thermotolerance, growth and amino acid metabolism under heat stress in broilers. *Animal* **14**, 1701–1709
48. Ito, K., Bahry, M., Hui, Y., Furuse, M., and Chowdhury, V. (2015) Acute heat stress up-regulates neuropeptide Y precursor mRNA expression and alters brain and plasma concentrations of free amino acids in chicks. *Comp. Biochem. Physiol. A. Mol. Integr. Physiol.* **187**, 13–19
49. Taki, M., Kajiwara, K., Yamaguchi, E., Sato, Y., and Yamaguchi, S. (2021) Fused thiophene-S,S-dioxide-Based super-photostable fluorescent marker for lipid droplets. *ACS Mater. Lett.* **3**, 42–49